

Cover Page

Title: [Evaluating Temporal and Spatial Variations in Vegetation Coverage in the Inner Mongolia Autonomous Region (2004-2023) Using *kNDVI*]

Author: [Zhang Wenjun]

Affiliation: [Inner Mongolia University of Science and Technology]

Date of Submission: [December 16, 2024]

Peer Review Status Statement

The peer review status of this preprint is as follows:

This document has been preliminarily reviewed and published on EarthArXiv with the DOI: <https://doi.org/10.31223/X5RB0P>.

Please note that this preprint has not yet undergone a full peer review process. Updated versions, if any, will include the updated status of peer review. Please feel free to contact any of the authors; we welcome feedback.

1 **Evaluating Temporal and Spatial Variations in Vegetation Coverage in the Inner Mongolia**
2 **Autonomous Region (2004-2023) Using *kNDVI***

3 Guangpu Wei^{1¶}, Wenjun Zhang^{2¶}, Zhiheng Zhu¹, Yaxian Gao², Xiaoyan Yu^{2*}

4 **Author information**

5 School of Architecture and Art Design, Inner Mongolia University of Science and Technology,
6 Baotou, Inner Mongolia, China

7 Guangpu Wei & Zhiheng Zhu

8 School of Economics and Management, Inner Mongolia University of Science and Technology,
9 Baotou, Inner Mongolia, China

10 Wenjun Zhang, Yaxian Gao & Xiaoyan Yu

11 Research Center of Industrial Informationization and Innovation in Inner Mongolia University
12 of Science and Technology, Baotou, Inner Mongolia, China

13 Wenjun Zhang, Yaxian Gao & Xiaoyan Yu

14 * Corresponding author

15 E-mail: yu_xiaoyan@imust.edu.cn

16 **Abstract:** The Inner Mongolia Autonomous Region (IMAR) is a crucial ecological zone in
17 China, facing significant environmental challenges, particularly climate change. To better
18 understand vegetation dynamics in this region, this study examines vegetation cover trends from
19 2004 to 2023 and identifies their driving factors using an innovative kernel-based Normalized
20 Difference Vegetation Index (*kNDVI*) dataset from MOD13Q1 V6.1 data in Google Earth Engine
21 (GEE). Spatiotemporal dynamics in vegetation cover were assessed using Theil-Sen median trend
22 analysis, the Mann-Kendall test, and the Hurst exponent. Additionally, correlation analyses explored
23 links between *kNDVI* and climate variables, including precipitation, temperature, and solar radiation
24 (srad). Results revealed a northeast-to-west gradient in vegetation cover, with 35.36% of vegetation
25 improving, 49.95% remaining stable, and 14.69% degrading. Future vegetation trends indicate
26 70.96% of the region has uncertain trajectories, while 29.04% shows potential for sustainable

27 development. Among the climatic factors influencing vegetation cover, precipitation was the
28 primary driver, followed by temperature and srad. Climatic factors were significant in western
29 Hulunbuir and central Ulanqab, whereas non-climatic factors, including human activities and land-
30 use changes, were dominant in Hulunbuir, Xing'an League, and Xilin Gol. These findings
31 underscore the necessity for region-specific ecological management strategies integrating climatic
32 and anthropogenic factors to enhance ecosystem resilience.

33 **Keywords:** spatiotemporal dynamics: vegetation cover: driving factors: ecological
34 management: the IMAR

35 Vegetation coverage is a critical indicator for assessing ecosystem health and tracking change
36 trends, and it has been widely applied in ecological monitoring and environmental assessment 1.
37 The grassland ecosystems of the Inner Mongolia Autonomous Region (IMAR) function as a key
38 ecological safeguard for China, with their growth directly affecting the stability and security of
39 regional ecosystems 2. In recent years, intensified climate change and anthropogenic activities have
40 resulted in significant spatio-temporal changes in the vegetation coverage across the IMAR 3. Most
41 existing studies, however, rely on localized data analyses and traditional vegetation indices such as
42 *NDVI*, which encounter challenges in the IMAR's arid and semi-arid environments including data
43 gaps and spatial inconsistencies, limiting monitoring accuracy 45. Therefore, a more precise
44 approach is urgently needed to address these challenges and enhance the accuracy and consistency
45 of large-scale vegetation monitoring 6.

46 Although numerous studies highlight the impact of climatic variables and anthropogenic
47 activities on vegetation dynamics, conventional vegetation indices face limitations in dry and semi-
48 arid locations, thereby hindering their effectiveness for precise monitoring 78. To address these

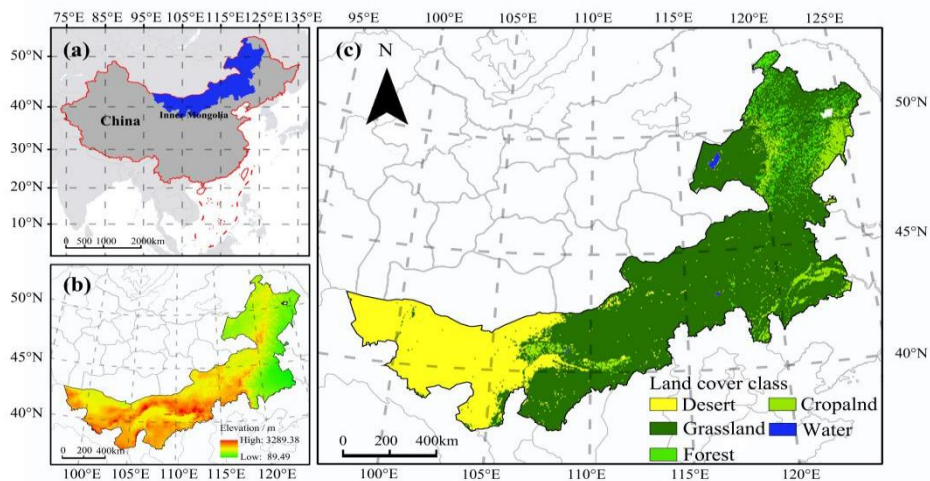
49 limitations, this research presents the kernel Normalized Difference Vegetation Index (*kNDVI*) as
50 the primary vegetation monitoring index. By employing kernel-based interpolation, *kNDVI* achieves
51 higher spatial continuity and consistency, enabling a more accurate reflection of the spatio-temporal
52 changes in vegetation cover in the IMAR 910. Additionally, to evaluate long-term stability and trends
53 in vegetation dynamics, the Hurst exponent is applied, which allows for the identification of
54 persistence and self-sustainability in vegetation coverage. This comprehensive approach aids in
55 predicting future vegetation trends and provides theoretical support for ecological management
56 111213.

57 This study uses MODIS remote sensing data from 2004 to 2023 to assess changes in vegetation
58 coverage and its spatial distribution in the IMAR based on the *kNDVI*. The study seeks to quantify
59 the impacts of climate factors and anthropogenic interventions on vegetation dynamics 1415. In
60 addition to providing an innovative technical approach for vegetation monitoring, this study offers
61 a scientific basis for formulating policies on ecological conservation and restoration 16. Through
62 the integration of *kNDVI*, this research significantly enhances the accuracy of vegetation monitoring
63 across large and complex ecological environments, demonstrating its significant potential and
64 innovative value 1718.

65 **1. Research Region**

66 The Inner Mongolia Autonomous Region (IMAR) ($37^{\circ}24' - 53^{\circ}23'N$, $97^{\circ}12' - 126^{\circ}04'E$), which
67 is located in China's north, covers approximately 1.183 million square kilometers. It consists of
68 seven distinct geomorphic units: the Alashan Plateau, Ordos Plateau, Inner Mongolian Plateau,
69 Hulunbuir Plateau, Hetao Plain, Greater Khingan Mountains, and Northeast Plain 19. The region
70 features a moderate continental monsoon climate, with temperatures and precipitation decreasing

71 from northeast to west. Additionally, solar radiation (srad) decreases from west to northeast. The
72 diverse vegetation types of this region are commonly referred to as “East Forest and West Mining,
73 South Grain and North Pastoral” 20. The primary ecosystem types in the IMAR include grassland,
74 woodland, desert, wetland, and sandy terrain, all of which play a crucial role in sustaining the local
75 ecological equilibrium 21.



76
77 **Figure 1.** The study area (a) geographical position of the IMAR in China; (b) elevation
78 distribution; (c) landscape types.
79

80 **2. Methodology**

81 **2.1. Data Acquisition and Processing**

82 The vegetation coverage data of the IMAR were gathered from the MOD13 Q1 V6.1 dataset
83 (<https://developers.google.com/>). The data had a 250-meter of space resolution and were collected
84 every 16 days. Annual *kNDVI* images from 2004 to 2023 were generated by computing *NDVI* data
85 on a pixel-by-pixel basis using the GEE platform. The *kNDVI* calculation technique was utilized to
86 evaluate vegetation dynamics over a 20-year span, providing significant insights into regional
87 vegetation patterns and alterations. The *kNDVI* calculation formula is provided below:

88
$$kNDVI = \tanh \left[\left(\frac{NIR - red}{2\sigma} \right)^2 \right]$$

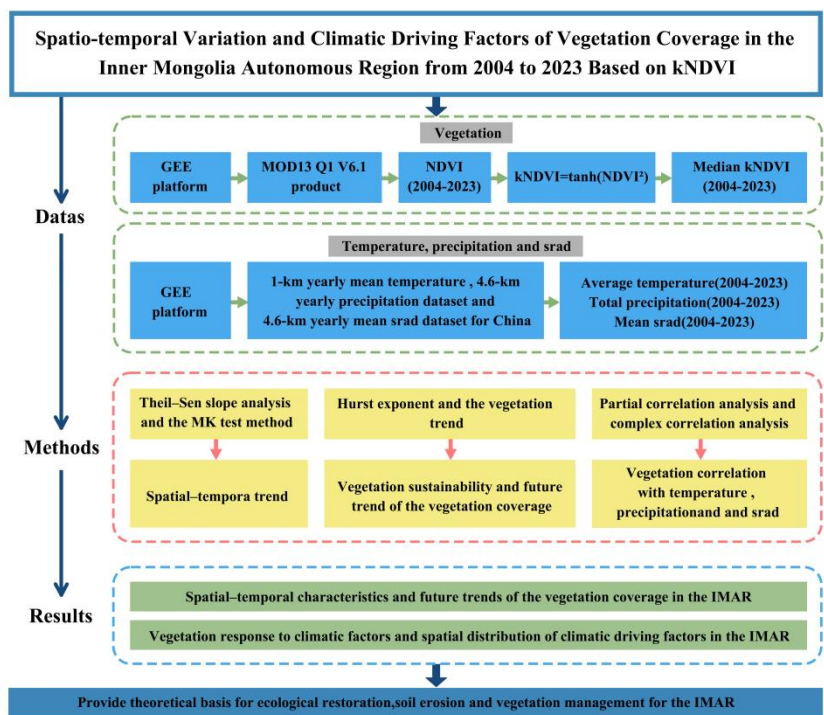
89 In the formula, the length scale parameter is designated for each unique application, indicating
90 the index's sensitivity to sparse or thick vegetation areas; NIR refers to the near-infrared spectrum;
91 Red denotes the red-light band; tanh represents the hyperbolic tangent function. An appropriate
92 option is to calculate the mean:

93
$$kNDVI = \tanh (NDVI^2)$$

94 The temperature data employed in this investigation were obtained from the MOD11 A2 V6.1
95 average temperature dataset (<https://developers.google.com>). This dataset possesses a geographical
96 resolution of 1,000 meters and updates at 8-day intervals. The precipitation and srad data were
97 obtained from the IDAHO_EPSCOR/TERRACLIMATE dataset (<https://developers.google.com>),
98 with a geographical resolution of 4.6 kilometers and a temporal resolution of 30 days. Utilizing the
99 GEE platform (<https://earthengine.google.com>), we computed the average temperature, total
100 precipitation, and mean srad from 2004 to 2023, and downloaded 20 images of temperature,
101 precipitation, and srad for the same period. Additionally, the vector boundary data originated from
102 the Resource and Environmental Science Data Platform (<https://www.resdc.cn>). The elevation data,
103 which were obtained from the National Oceanic and Atmospheric Administration
104 (<https://www.nci.noaa.gov>), have a spatial resolution of 30 meters. Furthermore, land classification
105 data were obtained from the Aerospace Information Innovation Research Institute under the Chinese
106 Academy of Sciences (<http://www.aircas.cn>), featuring a spatial resolution of 30 meters. Before
107 further analysis, all data were resampled to ensure consistency in both spatial and temporal
108 resolutions.

109 **2.2. Methods**

110 The pattern of vegetation change was analyzed through Theil-Sen slope and the Mann-Kendall
 111 (MK) tests, using *kNDVI* and climatic data. To evaluate vegetation dynamics' sustainability in
 112 grasslands, the Hurst index was applied. When integrated with partial and complex correlation
 113 analysis methods, it provided valuable insights into vegetation responses to climate conditions and
 114 their key drivers (Figure 2).



115

116 **Figure 2.** Workflow of the research process

117

118

119 **2.2.1. Examination of Spatial-Temporal Dynamics and Future Forecasts**

120 To analyze pixel-level vegetation trends over time, the Theil-Sen slope analysis and the MK
 121 test are often utilized in combination 222324. Theil-Sen slope analysis is recognized for its
 122 computational efficiency and robustness against measurement errors and discontinuous data 2526.
 123 Consequently, it was utilized to evaluate pixel-level *kNDVI* trends across the grasslands of IMAR

124 from 2004 to 2023. Besides, to assess the statistical significance of vegetation trends, we employed
 125 the MK test, which is advantageous since it does not necessitate a certain distribution for the sample,
 126 reduces the impact of outliers, and does not require a stringent linear trend 2728. This testing
 127 methodology is extensively employed to assess the significance of patterns in longitudinal data
 128 sequences2930.

129 The integration of $kNDVI$ trends with the Hurst exponent enables the forecasting of future
 130 vegetation trends 3132. This research divides the Hurst index value (H) into three categories: When
 131 $H > 0.5$, the $kNDVI$ time series shows a trend consistent with its future trends; For $H = 0.5$, the
 132 $kNDVI$ time series is classified as a random process lacking sustainability; when $H < 0.5$, it is
 133 considered unsustainable, suggesting a reverse trend in future $kNDVI$ time series 3334. The formulas
 134 for S_{kNDVI} and Z_S are presented below:

$$S_{kNDVI} = \text{Median} \left(\frac{kNDVI_j - kNDVI_i}{j - i} \right), 2004 \leq i < j \leq 2023 \quad (3)$$

$$Z_S = \begin{cases} \frac{S - 1}{\sqrt{\text{var}(S')}} S > 0; \\ 0, S = 0 \\ \frac{S + 1}{\sqrt{\text{var}(S')}} S < 0; \end{cases} \quad (4)$$

135

$$\text{Where, } S = \sum_{i=1}^{n-1} \sum_{j=i+1}^n \text{sgn}(x_j - x_i)$$

$$\text{Var}(S) = \frac{n(n-1)(2n+5) - \sum_{i=1}^m t_i(t_i-1)(2t_i+5)}{18}$$

136 S_{kNDVI} denotes the slope value calculated using the Theil-Sen method, and in the equations,
 137 $kNDVI_i$ denotes the $kNDVI$ value at pixel i , and $kNDVI_j$ denotes the value at pixel j ; the Z_S parameter
 138 ranges from $(-\infty$ to $+\infty)$; Z denotes the standardized test value; sgn indicates the sign function; n
 139 denotes the length of the $kNDVI$ time series; m stands for the count of repeated datasets; and t_i
 140 denotes the number of repetitions within the interval. At a significance level α , if $|Z_S| > u_{1-\alpha/2}$, it

141 implies substantial changes in the time series. In this investigation, we adopted the standard
142 significance level of $\alpha = 0.05$ to assess the pixel-level significance of *kNDVI* trends.

143 **2.2.2. Analysis of Driving Factors**

144 Partial correlation analysis was employed to investigate the relationships between *kNDVI* and
145 climatic variables, including average temperature, total precipitation, and mean *srad*, in the IMAR
146 from 2004 to 2023. The partial correlation coefficient (PCC) quantifies how strongly climatic factors
147 influence vegetation. The significance of the PCC was then assessed with a *t*-test. Furthermore, we
148 investigated the synergistic impacts of temperature, precipitation and *srad* on *kNDVI* through
149 correlation analysis. Finally, to evaluate the association between *kNDVI* and the combined effects
150 of temperature, precipitation, and *srad*, we computed the complex correlation coefficient (CCC) and
151 assessed its significance using an F-test 3536.

152 Given the regional variations in the PCC and CCC between *kNDVI* and climatic variables, we
153 utilized *t*-tests and F-tests to map and synthesize the spatial distribution of climatic driving factors
154 affecting vegetation change in the IMAR. To ensure optimal consistency and regional continuity
155 within each classification, the pixels satisfying the F-test criterion at a significance level of $\alpha =$
156 0.05 were selected for further climate-driven spatial categorization, while those pixels not meeting
157 this criterion were considered to be influenced by non-climatic factors. Utilizing the outcomes from
158 comparing *kNDVI* with each climatic parameter, we classified the climatic driving factors into three
159 distinct groups. The classification method is widely adopted as a determinant for vegetation cover
160 3738. The classification criteria are presented in Table 1.

161 **Table 1.** Criteria for classifying climatic driving forces influencing dynamic variations in *kNDVI*

Type of Driving Factor	Classification Basis
------------------------	----------------------

	$R_{kNDVI-P}$	$R_{kNDVI-T}$	$R_{kNDVI-S}$	$R_{kNDVI-T-P-S}$
Driven by precipitation	$ t >0.05$			$F>F_{0.05}$
Driven by temperature		$ t >0.05$		$F>F_{0.05}$
Driven by srad			$ t >0.05$	$F>F_{0.05}$
Driven by temperature, precipitation and srad	$ t <0.05$	$ t <0.05$	$ t <0.05$	$F>F_{0.05}$
Driven by non-climate factors				$F<F_{0.05}$

162 **Note:** $R_{kNDVI-P}$, $R_{kNDVI-T}$ and $R_{kNDVI-S}$ represent the PCC between $kNDVI$ and precipitation,
163 temperature, and srad, respectively; $R_{kNDVI-P-T-S}$ denotes the CCC between $kNDVI$ and the combined
164 climatic variables (precipitation, temperature, and srad); $t_{0.05}$ indicates that the correlation is significant
165 at the 0.05 level according to the t -test; $F_{0.05}$ signifies that the correlation is significant at the 0.05 level
166 based on the F-test.

167

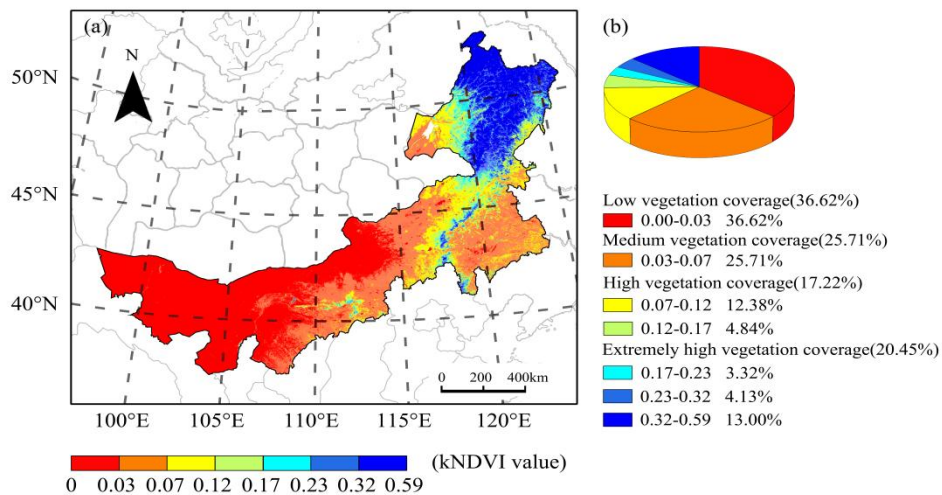
168 **3. Result**

169 **3.1. Spatial and Temporal Characteristics of $kNDVI$**

170 **3.1.1. Spatial Patterns of Vegetation Coverage**

171 The geographical distribution of the median $kNDVI$ in the IMAR over the past two decades,
172 based on $kNDVI$ median data from 2004 to 2023, is depicted in **Figure 3a**. The spatial distribution
173 of $kNDVI$ in the IMAR, as shown in the figure, indicates significantly higher vegetation coverage
174 in the northeast, diminishing towards the west. The mean $kNDVI$ across the region was 0.109, with
175 a variation range from 0 to 0.59. The mean $kNDVI$ values for the western, central, and northeastern
176 regions of the IMAR were 0.01, 0.05, and 0.26, respectively. Compared to the western region, the
177 $kNDVI$ values in the central and northeastern areas of the IMAR were higher. **Figure 3b** shows the
178 statistical categorization outcomes of the median $kNDVI$ and the distribution of each group
179 throughout the 20-year period in the IMAR, utilizing the natural break point approach. The largest
180 proportion of $kNDVI$ values below 0.3 was seen in the IMAR, indicating limited vegetation coverage,

181 mostly located in susceptible regions of the Alashan Plateau, Ordos Plateau, Hetao Plain, and the
 182 Inner Mongolian Plateau. Areas with $kNDVI$ values between 0.03 and 0.07, representing median
 183 vegetation coverage, were predominantly located in southern Ulanqab, eastern Chifeng, the entirety
 184 of Tongliao, and western Hulunbuir. Areas with $kNDVI$ values between 0.07 and 0.17 and those
 185 exceeding 0.17 were classified as having high and extremely high vegetation coverage, respectively.
 186 These regions primarily encompassed most of Hulunbuir, central Ulanqab, Xing'an League,
 187 Chifeng, and parts of Tongliao.



188

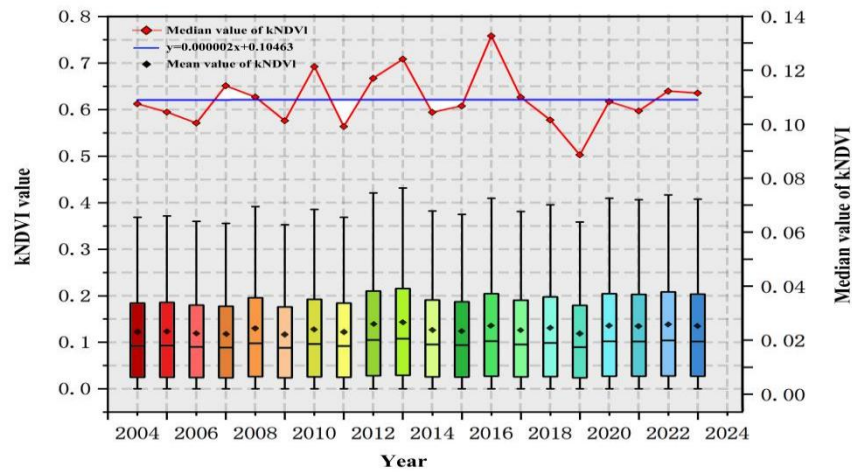
189 **Figure 3.** Geographical patterns and classification of vegetation cover: (a) median $kNDVI$
 190 from 2004 to 2023 in the IMAR (b) proportional distribution of each vegetation grouping

191

192 3.1.2. Temporal Dynamics of Vegetation Coverage

193 To investigate the temporal dynamics of $kNDVI$ across the IMAR, annual median $kNDVI$ values
 194 from 2004 to 2023 were employed to represent the overall vegetation condition for each year. **Figure**
 195 4 displays a box plot summarizing the yearly distribution of $kNDVI$ values, along with a line graph
 196 that illustrates the year-to-year fluctuations in median $kNDVI$ throughout the study period. The
 197 $kNDVI$ values in the IMAR exhibit a consistent trend with a variation rate of 0.011 every five years.

198 The *kNDVI* values demonstrate significant fluctuations annually. The *kNDVI* values in the IMAR
 199 range from 0.089 to 0.133. The peak value was 0.133 in 2016, while the nadir was 0.089 in 2019.



200
 201 **Figure 4.** Annual variations of median *kNDVI* in IMAR (2004–2023). The box plots depict the
 202 annual distribution of *kNDVI* values (left axis), while the line graph shows the median *kNDVI* for each
 203 year (right axis).

205 3.1.3. Characteristics of Spatial Variation in Vegetation Coverage

206 The spatial patterns of *kNDVI* variation across the IMAR (2004–2023) were analyzed using
 207 Mann-Kendall tests and the Theil-Sen slope analysis. Since no pixels exhibited an S_{kNDVI} value of
 208 zero, we adapted classification methods from previous studies to develop our approach 3940,
 209 resulting in the following classifications based on actual S_{kNDVI} conditions. We classified pixels into
 210 three categories based on their S_{kNDVI} values: stable vegetation areas (pixels with S_{kNDVI} values
 211 between -0.0005 and 0.0005), areas of vegetation increase (pixels with S_{kNDVI} values greater than
 212 or equal to 0.0005, $S_{kNDVI} \geq 0.0005$), and regions of vegetation degradation (pixels with S_{kNDVI}
 213 values less than or equal to -0.0005, $S_{kNDVI} \leq -0.0005$).

214 To determine the statistical significance of the *kNDVI* trends at each pixel, we applied the
 215 Mann-Kendall (MK) test using a confidence level of 0.05. A test result (Z_S) exceeding 1.96 or falling

216 below -1.96 indicates a significant change. If $-1.96 < Z_s < 1.96$, the alteration is deemed negligible.
 217 By applying the Theil-Sen slope analysis in conjunction with the Mann-Kendall (MK) test, we
 218 mapped the pixel-level spatial distribution of annual *kNDVI* trends across the IMAR. As presented
 219 in Table 2, the results were classified into five distinct categories, and the proportion of region for
 220 each category was calculated accordingly. Regions showing increased vegetation coverage
 221 constituted 35.36% of the total, while those maintaining stable vegetation made up 49.95%.
 222 Conversely, regions with reduced vegetation coverage constituted 14.69%.

223 **Table 2.** Results of statistical study on *kNDVI* trends

S_{KNDVI}	Z_s Value	<i>kNDVI</i> Trends	Area Percentage/%
≥ 0.0005	≥ 1.96	Significantly improved	18.90
≥ 0.0005	-1.96-1.96	Slightly improved	16.46
-0.0005—0.0005	-1.96-1.96	Stable	49.95
≤ -0.0005	-1.96-1.96	Slightly degraded	11.38
≤ -0.0005	≤ -1.96	Severely degraded	3.31

224 **Note:** Pixels with S_{KNDVI} values ranging from -0.0005 to 0.0005, and Z_s statistics satisfying $|Z_s| \geq$
 225 1.96, were classified as stable vegetation regions.

226
 227 Between 2004 and 2023 in the IMAR, the areas where vegetation coverage decreased were
 228 substantially more widespread than those where it increased, as shown in **Figure 5**. Regions with
 229 diminished vegetation coverage were predominantly situated in the eastern and western portions of
 230 Hulunbuir, Xing'an League, Tongliao, Chifeng, eastern Xilingol, southern Ulanqab, southeastern
 231 Ordos, southern Bayannur, and some parts in Hohhot and Baotou. The stable vegetation zones were
 232 mostly located in Alxa, northern Bayannur, northern Baotou, Ulanqab, western Xilingol, and
 233 western Hulunbuir. The region exhibiting an increase in vegetation coverage was limited, mostly in
 234 the middle and northern sectors of Hulunbuir, with minor extensions in Ulanqab, Chifeng, Xilingol,
 235 and Bayannur.

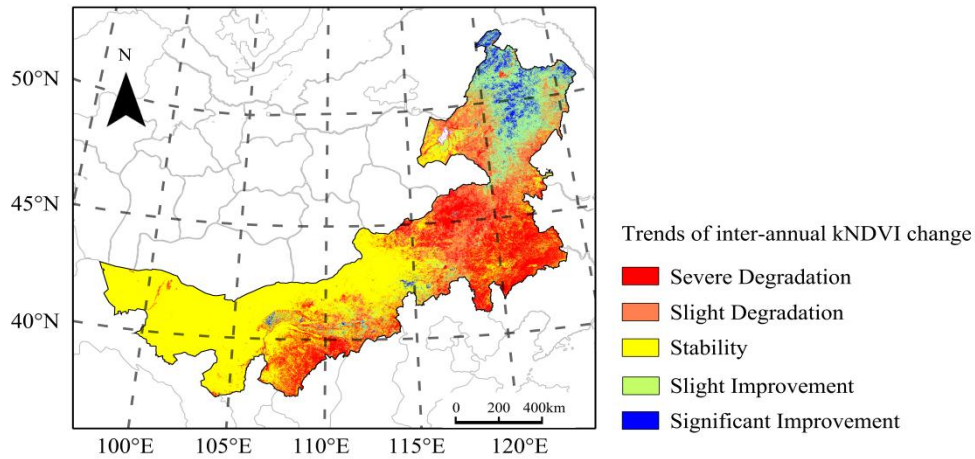


Figure 5. Annual variations of *kNDVI* in the IMAR from 2004 to 2023

236

237

238

239

240 3.1.4. Emerging patterns of Vegetation Coverage in the IMAR

241 In the IMAR, the average H value of *kNDVI* was determined to be 0.371, with 75.7% of the

242 regions exhibiting H values below 0.5, as shown in Figure 6a. This suggests that vegetation coverage

243 changes in most regions follow a periodic or gradually declining trend, with a degree of negative

244 long-term memory. Conversely, 24.3% of the regions exhibited H values exceeding 0.5, indicating

245 that in these areas, the trends in vegetation coverage were more persistent and demonstrated

246 favorable long-term memory. This suggests significant durability of the *kNDVI* in the IMAR. To

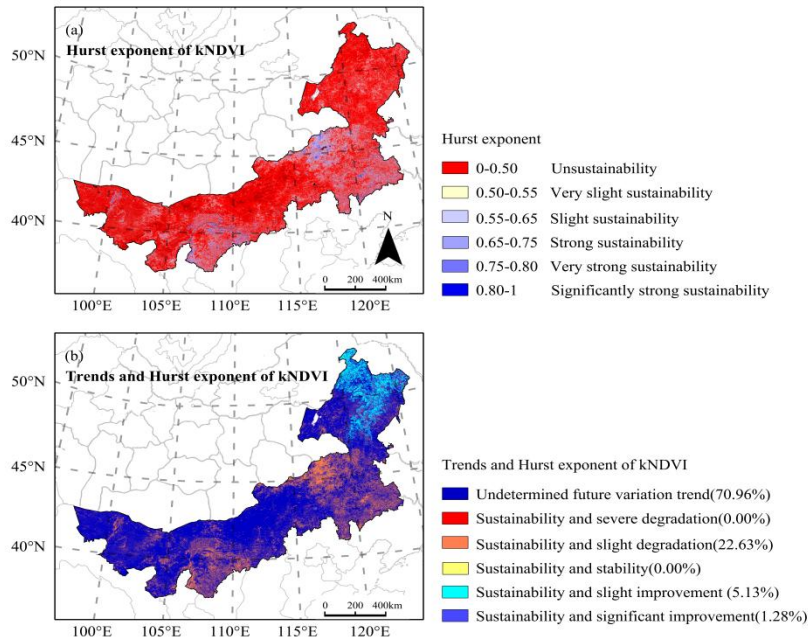
247 clarify the heterogeneity of vegetation trends and their sustainability, we combined the shifting

248 trends of *kNDVI* with the corresponding H values. This approach enabled us to extract coupling

249 information between trend dynamics and sustainability. As presented in **Figure 6b**, six distinct

250 scenarios derived from the coupling results. Notably, regions with H values below 0.5 from 2004 to

251 2023, regardless of the nature of *kNDVI* trends, were classified as having uncertain future trends.



252 Figure 6. Patterns of the Hurst exponent and projected vegetation dynamics: (a) map
 253 depicting the variation of the Hurst exponent across the region (b) map illustrating the anticipated
 254 future trends of *kNDVI*, based on current *kNDVI* changes and their sustainability.
 255

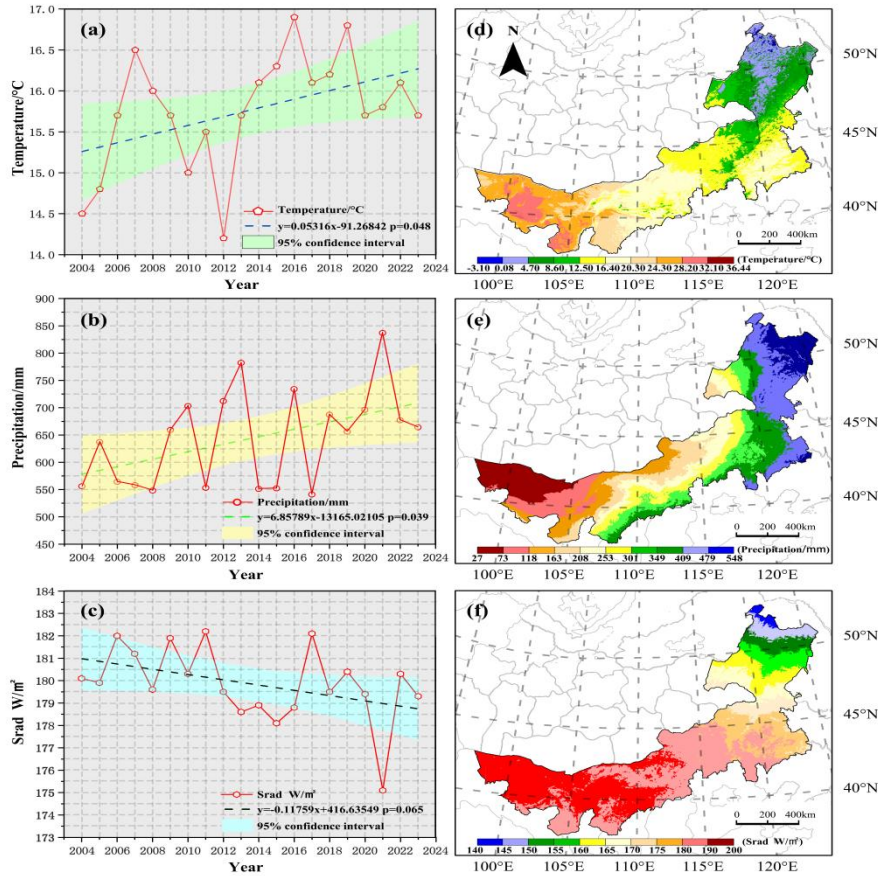
256

257 As illustrated in **Figure 6b**, the IMAR displays varied regional distributions of projected
 258 *kNDVI* trends. Areas classified as exhibiting “sustainability and improvement” comprised 6.41% of
 259 the total region, predominantly situated in the central and northern parts of Hulunbuir, with a smaller
 260 fraction extending into Xing’an League. The ratio of regions designated as “sustained stability” and
 261 “sustained severe degradation” was 0.22. Nevertheless, 63% of the overall region showed “sustained
 262 and slight degradation”. These areas were chiefly distributed across the Northeast Plain, the southern
 263 reaches of the Greater Khingan Range, the eastern sector of Inner Mongolia’s plateau, the Hetao
 264 Plain, and the Ordos Plateau, with a minor extension into the Alashan Plateau. Regions with
 265 uncertain future trends constituted 70.96%, predominantly located in the western and eastern sectors
 266 of Hulunbuir, Xilingol, Bayannur, and Alxa.

267 3.2. Factors Influencing Vegetation Coverage

268 3.2.1. Spatiotemporal Dynamics Patterns of Climatic Factors

269 Temporal variations in climatic variables across the IMAR from 2004 to 2023 were examined
270 by extracting pixel-level data on temperature, precipitation, and srad from images representing the
271 average temperature, total precipitation, and mean srad. Leveraging these datasets, we characterized
272 the general climatic patterns on a yearly basis. The analysis of the average temperature, precipitation,
273 and srad data from 2004 to 2023 illustrates the regional distribution characteristics of the IMAR's
274 climate. **Figures 7a–c** revealed that temperature, precipitation, and srad throughout IMAR had
275 generally exhibited upward trends with fluctuations. These findings are crucial for restoring
276 ecosystems and promoting sustainable progress within the IMAR. In the IMAR, the annual average
277 temperature increased by approximately 0.3 °C/5a, total annual precipitation by 27 mm/5a, and the
278 annual mean srad by 0.525 W/m². Consequently, the climate in the IMAR demonstrated a clear
279 pattern of rising temperature and humidity. To reveal the spatial patterns of temperature,
280 precipitation, and srad, we applied a statistical classification method to divide these variables into
281 ten distinct categories. **Figures 7d–f** illustrate that from 2004 to 2023, the IMAR had an average
282 temperature of 16.36°C, total average precipitation of 274.1 mm, and mean srad of 180.03 W/m².
283 The temperature exhibited geographic variation, fluctuating between -3.1°C and 36.44°C from
284 northeast to west. Precipitation varied from 27 to 556 mm, with an increase from the west to the
285 northeast. The srad steadily decreased from west to northeast, ranging from 139.46 to 199.27 W/m².
286 Moreover, there was significant geographical diversity in temperature, precipitation, and srad across
287 the IMAR.



288

289 **Figure 7.** Temporal trends and spatial distributions of climatic variables in IMAR (2004–2023): (a)
 290 temporal variations in average temperature (b) temporal variations in total precipitation (c) temporal
 291 variations in mean srad (d) spatial patterns of average temperature distribution (e) spatial patterns of
 292 total precipitation distribution (f) spatial patterns of mean srad distribution.

293

294 3.2.2. Analysis of Partial Correlations Between *kNDVI* and Climatic Variables

295 Employing the breakpoint method, we classified the regional patterns of partial correlation

296 coefficients (PCC) between *kNDVI* and climatic factors. Between 2004 and 2023, the PCC relating

297 *kNDVI* to temperature ranged from -1 to 1, with an average of -0.11 (**Figure 8a**). Pixels exhibiting

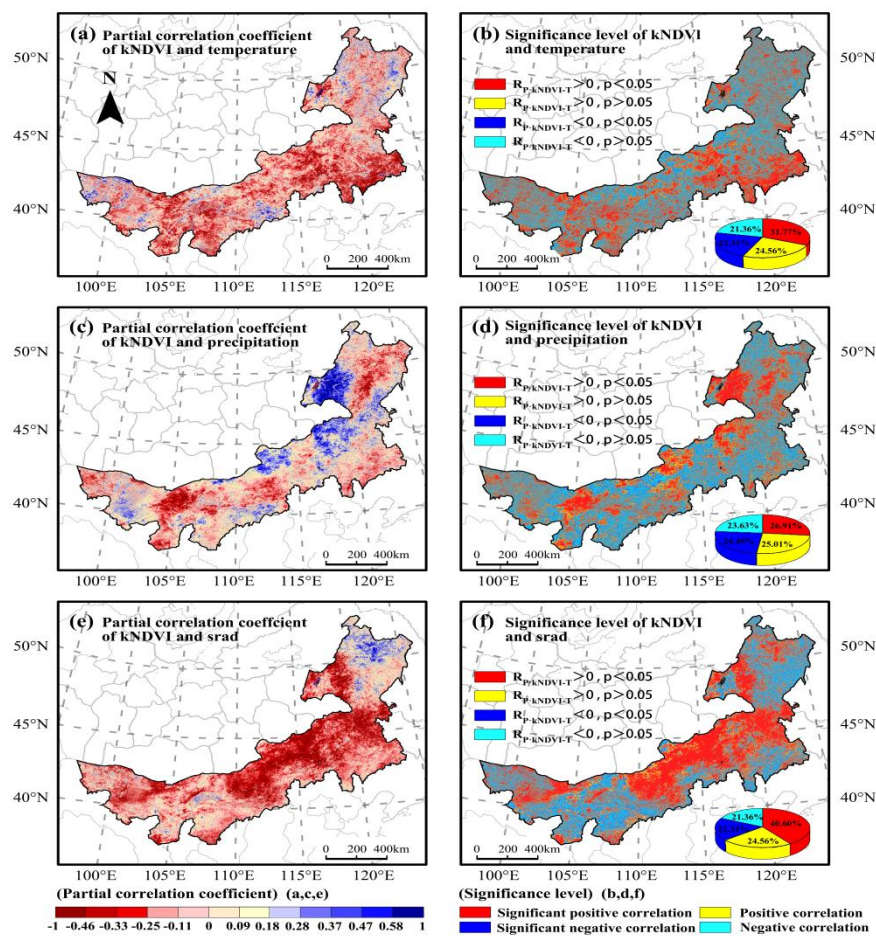
298 positive correlation (56.33%) were more prevalent than those demonstrating negative correlation

299 (43.67%), with 31.77% categorized as “significantly positively correlated” and 22.31% as

300 “significantly negatively correlated” (**Figure 8b**). The results demonstrated significant variation in

301 the regional distribution pattern of PCC across *kNDVI* and temperature. The pixels with a strong

302 positive correlation were predominantly located in central Xilingol, southern Chifeng and Tongliao,
 303 western Ordos, and eastern Alxa. In contrast, negatively correlated pixels were predominantly
 304 located in the northeast and south of Hulunbuir, throughout most of Xing'an League, northern
 305 Tongliao, Ulanqab, southern Hohhot, the majority of Bayannur, southern Ordos, and western and
 306 southern Alxa League. Pixels with significant negative correlation were primarily observed in
 307 Hulunbuir, Xing'an League, Xilingol, Hohhot, and Ordos.



308
 309 **Figure 8.** Spatial analysis of PCC and significance levels between *kNDVI* and climatic factors: (a)
 310 PCC between *kNDVI* and temperature, ($R_{kNDVI-T}$) (b) significance level corresponding to $R_{kNDVI-T}$
 311 (c) PCC between *kNDVI* and precipitation, ($R_{kNDVI-P}$) (d) significance level corresponding to
 312 $R_{kNDVI-P}$ (e) PCC between *kNDVI* and srad, ($R_{kNDVI-S}$) (f) significance level corresponding to
 313 $R_{kNDVI-S}$

314

315 From 2004 to 2023, the PCC between *kNDVI* and precipitation spanned the entire range from

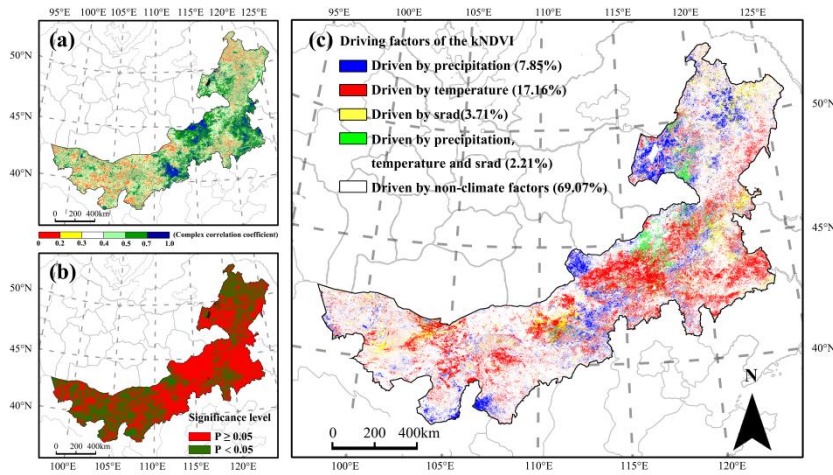
316 -1 to 1, averaging 0.02 (**Figure 8c**). Pixels with positive correlation constituted 51.92%, whilst those
317 with negative correlation comprised 48.08%. **Figure 8d** demonstrates that the pixels with a strong
318 positive correlation were primarily situated in the western region of Hulunbuir, the eastern region
319 of Xilingol, the central region of Ulanqab, and along the boundary between Alxa and Bayannur. The
320 pixels exhibiting significant negative correlation and negative correlation were predominantly
321 distributed across eastern and northern regions of Hulunbuir, Xing'an League, Chifeng, Tongliao,
322 central Xilingol, northern Ulanqab, Baotou, Hohhot, the majority of Ordos, eastern and northern
323 Bayannur, and most of Alxa.

324 The PCC between *kNDVI* and *srad* spanned the entire possible range, with an average of -0.18
325 (**Figure 8e**). Positive correlations were observed in 65.16% of the pixels, surpassing the 34.84%
326 that showed negative correlations. **Figure 8f** demonstrates that significant positive correlations were
327 primarily identified in western Hulunbuir, eastern Xilingol, central Ulanqab, and along the boundary
328 between Bayannur and Alxa. Significant negative and negative correlations were predominantly
329 observed in eastern and northern Hulunbuir, Xing'an League, Chifeng, Tongliao, central and
330 western Xilingol, northern Ulanqab, Baotou, Hohhot, most of Ordos, northern Bayannur, and much
331 of Alxa. The vegetation in the IMAR exhibited a pronounced sensitivity to climatic conditions,
332 ranked in influence as follows: precipitation, temperature, and *srad*.

333 **3.2.3. Examination of Determinants Influencing Vegetation Coverage**

334 Applying the breakpoint method, we categorized the cross-correlations between *kNDVI* and
335 climatic variables, as depicted in **Figure 9a**, with their significance levels shown in **Figure 9b**.

336 Within the IMAR, these correlations exhibited a broad range and averaged 0.44. Notably, only 32.5%
337 of the pixels demonstrated statistically significant correlations at the 0.05 level.



338
 339 **Figure 9.** Determinants of *kNDVI* Analysis: (a) regional distribution of the CCC between *kNDVI*
 340 and climatic variables (b) significance levels of the CCC (c) factors influencing *kNDVI* in the
 341 IMAR (2004-2023)

342
 343 Analyzing correlations from 2004 to 2023 revealed spatiotemporal variability within the IMAR.

344 The vegetation patterns, influenced by climatic conditions, were categorized into distinct zones.

345 **Figure 9c** depicts the regional distribution of these driving forces. The findings revealed that only

346 30.93% of the vegetation coverage in the IMAR was influenced by climatic variables, whereas 69.07%

347 was influenced by non-climatic factors. Climatic factors, specifically precipitation, influenced 7.85%

348 of the regions, predominantly in Hulunbuir, western Xilingol, southern Ulanqab, southwestern

349 Ordos, and southern Alxa. The temperature-driven zone covered 17.16% of the area, primarily

350 situated in the eastern region of Alxa and the northern sections of Ordos, Baotou City, Ulanqab,

351 Xilingol, Chifeng, southern Tongliao, Xing'an League, and both eastern and western parts of

352 Hulunbuir. The srad-driven area constituted 3.71%, primarily distributed in northern Hulunbuir,

353 eastern Xing'an League, and central Ulanqab, Baotou City, and Alxa. The region affected by

354 temperature, precipitation, and srad accounted for 2.21% of the total, predominantly located in the

355 western half of Hulunbuir, the western section of Xing'an League, and the central-eastern zone of

356 Xilingol. Our findings suggest that in the IMAR, vegetation was predominantly influenced by non-
357 climatic factors, and this influence was observed across many cities throughout the region.

358 **4. Discussion**

359 **4.1. Temporal Evolution and Spatial Distribution of *kNDVI***

360 From 2004 to 2023, we investigated the temporal and spatial variations of *kNDVI* across the
361 IMAR. The analysis revealed that vegetation coverage was notably higher in the northeastern region
362 (**Figure 3a**), likely due to humid climatic conditions, ample precipitation, and the presence of
363 wetland ecosystems 4142. The predominant plant type was grassland, with the exception of trees
364 and bushes. By contrast, the biological habitat in the western region, which was predominantly
365 influenced by environmental variables 43 was more fragile, as indicated by the low *kNDVI* values.
366 This fragility was particularly evident in areas such as Alxa. Alxa hosts the expansive Badain Jaran
367 Desert, covering approximately 49,000 square kilometers and recognized as one of China's largest
368 deserts. Similarly, the Tengger Desert in Alxa Left Banner extends over 43,000 square kilometers,
369 ranking among the country's most extensive desert regions. Additionally, the Kubuqi Desert and
370 Ulanbuhe Desert, which cover smaller area, are situated to the west of the IMAR 44.

371 In comparison to other research, vegetation coverage data exhibited a consistent and declining
372 trend overall (**Figure 4**). The "stable" vegetation coverage category was the predominant one in the
373 IMAR, although the "uncertain future trend" category also represented a significant portion (**Figure**
374 **5 and Figure 6b**). The prevalence may be attributed to the influence of various factors on surface
375 vegetation changes, such as climate change, alterations in land use, and human activities, with their
376 interactions potentially being complex, resulting in uncertainty about future trends 4546.

377 Nonetheless, the percentage of "sustainable and slightly degraded" regions was also notably

378 high, indicating “very strong sustainability”, which implies that vegetation coverage in the IMAR
379 has likely experienced a minor decline in the recent past and may continue to decline in the
380 foreseeable future. This is mostly due to natural factors, human activities, or other environmental
381 causes that negatively impact vegetation in these areas 47. Agriculture and animal husbandry have
382 consistently been foundational sectors in the IMAR, and overgrazing has caused grassland
383 degradation, leading to a notable reduction in vegetation cover. However, certain areas have
384 exhibited “sustainability and substantial enhancement”. This favorable advancement may be chiefly
385 ascribed to the government’s implementation of various ecological protection laws aimed at
386 increasing vegetation coverage and restoring the ecological environment. The government has
387 strengthened the protection of vegetative resources, including grasslands and forests, imposed
388 restrictions on development and logging, and implemented policies to convert cropland into forests
389 and grasslands 4849. Nevertheless, there has been a slight reduction in the overall vegetation across
390 the IMAR.

391 **4.2. Analysis of the Influencing Factors on *kNDVI***

392 The analysis revealed that non-climatic factors significantly influence vegetation in the IMAR
393 (**Figure 9c**), indicating that key drivers of *kNDVI* differ across regions 50. Prior studies have
394 identified anthropogenic activities, precipitation, temperature, and *srad* as the principal determinants
395 of vegetation coverage 51. In areas with minimal human impact, fluctuations in vegetation coverage
396 were primarily attributed to weather influences 52.

397 The investigation into the regional distribution of driving forces indicated notable spatial
398 variability in climatic variables throughout the IMAR. Most precipitation-dependent regions were
399 located in dry or semi-arid zones, where rainfall is often limited. Conversely, areas affected by

400 temperature tended to experience relatively low temperatures. Regions impacted by strong srad were
401 predominantly located in low-latitude zones with sparse vegetation, particularly those below 500
402 meters in elevation. Conversely, regions affected by a confluence of precipitation, temperature, and
403 srad were predominantly situated at elevated heights, especially in Xilingol, where the elevation
404 surpasses 1,000 meters. Geographical variations highlight the influence of height and topography
405 on climatic elements including temperature, moisture availability, and light, which directly impact
406 plant distribution 53. Therefore, areas which are susceptible to natural disasters should use tailored
407 strategies to improve resilience to cold and drought, based on their specific climate conditions.

408 Incorporating precipitation, temperature, and srad into vegetation management establishes a
409 robust foundation for enhancing plant development and sustaining ecological equilibrium. Effective
410 measures include careful consideration of local climatic and hydrological conditions to prevent
411 problems such as overplanting and excessive soil moisture loss. Customized and knowledgeable
412 strategies are essential for achieving sustainable vegetation management 54.

413 **4.3. Limitations and Guidelines for Subsequent Research**

414 This study analyses trends in vegetation change, assesses the long-term stability of vegetation
415 dynamics, and it also examines the influence of climatic factors on the spatial distribution of
416 vegetation in the IMAR. The findings of this study can facilitate the efficient monitoring of
417 vegetation alterations and provide a theoretical foundation for conservation and rehabilitation
418 initiatives in the IMAR.

419 Nevertheless, our study has several limitations. Firstly, although prospective vegetation
420 changes can be quantified by integrating *kNDVI* trends and H values, the Hurst index fails to offer
421 insights into the longevity of sustainable vegetation dynamics. Therefore, it is essential to develop

422 methodologies that can more accurately capture temporal patterns 55. Additionally, in some years,
423 the yearly median *kNDVI* values were very low, which allowed for the identification of interference
424 years and regions of vegetation coverage from 2004 to 2023. This limitation calls for further
425 examination of the factors affecting plant growth. Temperature, precipitation, and *srad* were
426 identified as major climate-related elements influencing vegetation coverage, yet the complex
427 interplay between these factors and topography at micro and macro scales could not be fully
428 captured 56. Lastly, several natural factors, such as soil composition and runoff, also affect
429 vegetation coverage, suggesting a need for more comprehensive data in future studies. Consequently,
430 further research should examine these natural factors that were not addressed in this study 57.

431 Moreover, non-climatic factors exert a significant influence on vegetation coverage in the
432 IMAR. Over time, the complexity of vegetation dynamics has been substantially affected by
433 anthropogenic activities such as urban expansion, infrastructure development, grazing, and changes
434 in land use and land cover (LUCC). Therefore, future research should focus on integrating these
435 anthropogenic variables into studies to better understand their geographical effects on vegetation 58.

436 **5. Conclusions**

437 In this study, calculations of *kNDVI* were performed on the GEE platform using MOD13Q1
438 V6.1 data. The annual median *kNDVI* values from 2004 through 2023 were utilized as indicators of
439 vegetation status for each respective year. We analyzed the spatiotemporal characteristics of *kNDVI*
440 across the IMAR by correlating it with temporal datasets of temperature, precipitation, and *srad*.
441 This approach revealed *kNDVI*'s sensitivity to climatic variables and other driving forces.

442 The findings indicated that vegetation coverage in the IMAR was substantially higher in
443 northeastern regions and decreased towards the west, exhibiting considerable spatial variability.

444 Specifically, the yearly median *kNDVI* varied between 0.089 and 0.133 from 2004 to 2023,
445 indicating a consistent trend. Over this period, 35.36% of vegetation coverage in the IMAR showed
446 improvement, 49.95% remained stable, and 14.69% experienced degradation. In terms of
447 sustainability, 70.96% of the vegetation coverage exhibited “unpredictable future trends”, while
448 29.04% was classified as sustainable, including 6.41% categorized as “sustainability and
449 improvement” and 22.63% as “sustainability and degradation”. Furthermore, vegetation coverage
450 was strongly influenced by climatic factors, ranked in order of influence as follows: precipitation,
451 temperature, and *srad*. At a 0.05 confidence level, non-climatic factors influenced 69.07% of the
452 vegetation, predominantly across much of Hulunbuir, Xing’an League, Ulanqab, Baotou, Hohhot,
453 Bayannur, Wuhai, and extensive areas of Alxa. In contrast, 30.93% of vegetation changes were
454 driven by climatic factors, mainly in the western Hulunbuir and Xing’an League, Xilingol, central
455 Ulanqab, central Baotou, and eastern Alxa. Overall, this study integrates *kNDVI* with various
456 analytical methods to offer a robust approach for monitoring vegetation dynamics in large-scale,
457 ecologically complex environments. The findings provide valuable scientific insights to support
458 ecological restoration and sustainable development efforts in the IMAR.

459 **Author Contributions:**

460 ¶ These authors contributed equally to this work.

461 Investigation, Methodology, and Analysis: G.W. and W.Z.; Supervision and Validation: X.Y.
462 and Z.Z.; Writing—Original Draft: W.Z.; Writing—Review and Editing: G.W. and Y.G. All authors
463 read and approved the final manuscript.

464 **Funding:**

465 Natural Science Foundation of Inner Mongolia Autonomous Region (2022LHMS07004).

466 **Ethical standards**

467 The experiments comply with the current laws of the country in which they were performed.

468 **Data Availability Statement:**

469 The data presented in this study can be obtained by contacting the corresponding author upon
470 request.

471 **Conflicts of Interest:**

472 The authors declare no conflicts of interest.

473 **References**

- 474 1. De Carvalho RM, Szlafsztein CF. Urban vegetation loss and ecosystem services: The influence on climate
475 regulation and noise and air pollution. *Environmental Pollution*. 2019, 245, 844-852.
- 476 2. Li S, Xie YC, Brown DG, Bai YF, Hua J, Judd K. Spatial variability of the adaptation of grassland vegetation
477 to climatic change in Inner Mongolia of China. *Applied Geography*. 2013, 43, 1-12.
- 478 3. Li JZ, Liu YM, Cao MM, Xue B. Space-Time Characteristics of Vegetation Cover and Distribution: Case of
479 the Henan Province in China. *Sustainability*. 2015, 7, 11967-11979.
- 480 4. Hu MM, Xia BC. A significant increase in the normalized difference vegetation index during the rapid
481 economic development in the Pearl River Delta of China. *Land Degradation & Development*. 2019, 30, 359-
482 370.
- 483 5. Gui X, Wang LC, Yao R, Yu DQ, Li CA. Investigating the urbanization process and its impact on vegetation
484 change and urban heat island in Wuhan, China. *Environmental Science and Pollution Research*. 2019,
485 26,30808-30825.
- 486 6. Propastin PA. 2009 Spatial non-stationarity and scale-dependency of prediction accuracy in the remote
487 estimation of LAI over a tropical rainforest in Sulawesi, Indonesia. *Remote Sensing of Environment*. 2009,

- 488 113, 2234-2242.
- 489 7. Guerschman JP, Hill MJ, Renzullo LJ, Barrett DJ, Marks AS, Botha EJ. Estimating fractional cover of
490 photosynthetic vegetation, non-photosynthetic vegetation and bare soil in the Australian tropical savanna
491 region upscaling the EO-1 Hyperion and MODIS sensors. *Remote Sensing of Environment*. 2009, 113, 928-
492 945.
- 493 8. Jjagwe P, Chandel AK, Langston D. Pre-Harvest Corn Grain Moisture Estimation Using Aerial Multispectral
494 Imagery and Machine Learning Techniques. *Land*. 2023, 12, 2188.
- 495 9. Gu Z, Chen X, Ruan W, Zheng M, Gen K, Li X, Deng H, Chen Y, Liu M. Quantifying the direct and indirect
496 effects of terrain, climate and human activity on the spatial pattern of *kNDVI*-based vegetation growth: A case
497 study from the Minjiang River Basin, Southeast China. *Ecological Informatics*. 2024, 80, 102493.
- 498 10. Yu H, Yang Q, Jiang S, Zhan B, Zhan C. Detection and Attribution of Vegetation Dynamics in the Yellow
499 River Basin Based on Long-Term Kernel *NDVI* Data. *Remote Sensing*. 2024, 16, 1280.
- 500 11. Peng J, Liu Z, Liu Y, Wu J, Han Y. Trend analysis of vegetation dynamics in Qinghai–Tibet Plateau using
501 Hurst Exponent. *Ecological Indicators*. 2012, 14, 28-39.
- 502 12. Wang J, Zhao J, Zhou P, Li K, Cao Z, Zhang H, Han Y, Luo Y, Yuan X. Study on the spatial and temporal
503 evolution of *NDVI* and Its Driving Mechanism Based on Geodetector and Hurst Indexes: a case study of the
504 Tibet Autonomous Region. *Sustainability*. 2023, 15, 5981.
- 505 13. Tran TV, Tran DX, Nguyen H, Latorre Carmona P, Myint SW. Characterising spatiotemporal vegetation
506 variations using *LANDSAT* time - series and Hurst exponent index in the Mekong River Delta. *Land*
507 *Degradation & Development*. 2021, 32, 3507-3523.
- 508 14. Li A, Wu J, Huang J. Distinguishing between human-induced and climate-driven vegetation changes: a critical
509 application of *RESTREND* in inner Mongolia. *Landscape ecology*. 2012, 27, 969-982.

- 510 15. Zhu L, Shi M, Fan D, Tu K, Sun W. Analysis of changes in vegetation carbon storage and net primary
511 productivity as influenced by land-cover change in inner Mongolia, China. *Sustainability*. 2023, 15, 4735.
- 512 16. Tian H, Cao C, Chen W, Bao S, Yang B. Myneni RB. Response of vegetation activity dynamic to climatic
513 change and ecological restoration programs in Inner Mongolia from 2000 to 2012. *Ecological Engineering*.
514 2015, 82, 276-289.
- 515 17. Guo B, Zhang R, Lu M, Xu M, Liu P, Wang L. A New Large-Scale Monitoring Index of Desertification Based
516 on Kernel Normalized Difference Vegetation Index and Feature Space Model. *Remote Sensing*. 2024, 16, 1771.
- 517 18. Wang Q, Moreno-Martínez Á, Muñoz-Mari J, Campos-Taberner M, Camps-Valls G. Estimation of vegetation
518 traits with kernel NDVI. *ISPRS Journal of Photogrammetry and Remote Sensing*. 2023, 195, 408-417.
- 519 19. Nanzad L, Zhang J, Tuvdendorj B, Yang S, Rinzin S, Prodhan FA, Sharma TP. Assessment of drought impact
520 on net primary productivity in the terrestrial ecosystems of Mongolia from 2003 to 2018. *Remote Sensing*.
521 2021, 13, 2522.
- 522 20. Fang J, Piao S, Tang Z, Peng C, Ji W. Interannual variability in net primary production and precipitation.
523 *Science*. 2001, 293, 1723.
- 524 21. Qi J, John R, Groisman P, Chen J. Understanding livestock production and sustainability of grassland
525 ecosystems in the Asian Dryland Belt. *Ecological Processes*. 2017, 6, 1-10.
- 526 22. Yeh HF, Yeh CF, Lee CH. Mann-Kendall test and Theil-Sen estimator for long-term spatial and temporal trends
527 of streamflow in Taiwan. *Journal of Chinese Soil and Water Conservation*. 2016, 47, 73-83.
- 528 23. Fensholt R, Proud SR. Evaluation of Earth Observation based global long term vegetation trends—Comparing
529 GIMMS and MODIS global NDVI time series. *Remote sensing of Environment*. 2012, 119, 131-147.
- 530 24. Li P, Wang J, Liu M, Xue Z, Bagherzadeh A, Liu M. Spatio-temporal variation characteristics of *NDVI* and its
531 response to climate on the Loess Plateau from 1985 to 2015. *Catena*. 2021, 203, 105331.

- 532 25. Xu T, Wu H. Spatiotemporal analysis of vegetation cover in relation to its driving forces in Qinghai–Tibet
533 Plateau. *Forests*. 2023, 14,1835.
- 534 26. Ay M, Kisi O. Investigation of trend analysis of monthly total precipitation by an innovative method.
535 *Theoretical and Applied Climatology*. 2015, 120, 617-629.
- 536 27. Bao G, Qin Z, Bao Y, Zhou Y, Li W, Sanjjav A. NDVI-based long-term vegetation dynamics and its response
537 to climatic change in the Mongolian Plateau. *Remote Sensing*. 2014, 6, 8337-8358.
- 538 28. AlSubih M, Kumari M, Mallick J, Ramakrishnan R, Islam S, Singh CK. Time series trend analysis of rainfall
539 in last five decades and its quantification in Aseer Region of Saudi Arabia. *Arabian Journal of Geosciences*.
540 2021, 14, 1-5.
- 541 29. Neeti N, Eastman JR. A contextual mann - kendall approach for the assessment of trend significance in image
542 time series. *Transactions in GIS*. 2011, 15, 599-611.
- 543 30. Güçlü YS. 2018 Multiple Şen-innovative trend analyses and partial Mann-Kendall test. *Journal of Hydrology*.
544 2018, 566, 685-704.
- 545 31. Zhao JP, Guo EL, Wang YF, Kang Y, Gu XL. Ecological drought monitoring of Inner Mongolia vegetation
546 growing season based on kernel temperature vegetation drought index (*kTVDI*). *Ying Yong Sheng tai xue bao*=
547 *The Journal of Applied Ecology*. 2023, 34, 2929-2937.
- 548 32. Chen Z, Zhang X, Jiao Y, Cheng Y, Zhu Z, Wang S, Zhang H. Investigating the spatio-temporal pattern
549 evolution characteristics of vegetation change in Shendong coal mining area based on *kNDVI* and intensity
550 analysis. *Frontiers in Ecology and Evolution*. 2023, 11, 1344664
- 551 33. Qiao X, Zhang J, Liu L, Zhang J, Zhao T. Spatiotemporal Changes in Vegetation Cover during the Growing
552 Season and Its Implications for Chinese Grain for Green Program in the Luo River Basin. *Forests*. 2024, 15,
553 1649.

- 554 34. Kang Y, Guo E, Wang Y, Bao Y, Bao Y, Mandula N. Monitoring vegetation change and its potential drivers in
555 Inner Mongolia from 2000 to 2019. *Remote Sensing*. 2021, 13, 3357.
- 556 35. Piao S, Fang J, Zhou L, Ciais P, Zhu B. Variations in satellite - derived phenology in China's temperate
557 vegetation. *Global change biology*. 2006, 12, 672-685.
- 558 36. Gao N, Zhou J, Zhang X, Cai W, Guan T, Jiang L, Du H, Yang D, Cong Z, Zheng Y. 2017 Correlation between
559 vegetation and environment at different levels in an arid, mountainous region of China. *Ecology and Evolution*.
560 2017, 7, 5482-5492.
- 561 37. Behjat V, Mahvi M, Rahimpour E. New statistical approach to interpret power transformer frequency response
562 analysis: non - parametric statistical methods. *IET Science, Measurement & Technology*. 2016, 10, 364-369.
- 563 38. Feng X, Tian J, Wang Y, Wu J, Liu J, Ya Q, Li Z. Spatio-temporal variation and climatic driving factors of
564 vegetation coverage in the Yellow River Basin from 2001 to 2020 based on *kNDVI*. *Forests*. 2023, 14, 620.
- 565 39. Ahmed SM. Assessment of irrigation system sustainability using the Theil–Sen estimator of slope of time
566 series. *Sustainability science*. 2014, 9, 293-302.
- 567 40. Some'e BS, Ezani A, Tabari H. Spatiotemporal trends and change point of precipitation in Iran. *Atmospheric*
568 *research*. 2012, 113, 1-2.
- 569 41. Piao S, Fang J, Ciais P, Peylin P, Huang Y, Sitch S, Wang T. The carbon balance of terrestrial ecosystems in
570 China. *Nature*. 2009, 458, 1009-1013.
- 571 42. Zhang X, Hu Y, Zhuang D, Qi Y, Ma X. *NDVI* spatial pattern and its differentiation on the Mongolian Plateau.
572 *Journal of geographical sciences*. 2009, 19, 403-415.
- 573 43. Li D, Liu K, Wang S, Wu T, Li H, Bo Y, Zhang H, Huang Y, Li X. Four decades of hydrological response to
574 vegetation dynamics and anthropogenic factors in the Three-North Region of China and Mongolia. *Science of*
575 *The Total Environment*. 2023, 857, 159546.

- 576 44. Wang M, Dong Z, Luo W, Lu J, Li J. Spatial variability of vegetation characteristics, soil properties and their
577 relationships in and around China's Badain Jaran Desert. *Environmental Earth Sciences*. 2015, 74, 6847-6858.
- 578 45. Zhang Y, Wang Q, Wang Z, Yang Y, Li J. Impact of human activities and climate change on the grassland
579 dynamics under different regime policies in the Mongolian Plateau. *Science of the Total Environment*. 2020,
580 698, 134304.
- 581 46. He D, Huang X, Tian Q, Zhang Z. Changes in vegetation growth dynamics and relations with climate in inner
582 Mongolia under more strict multiple pre-processing (2000–2018). *Sustainability*. 2020, 12, 2534.
- 583 47. Kuan CH, Chenchen YA, Liga BA, Yu CH. Rui LI, Luomeng, C.H. Effects of natural and human factor on
584 vegetation normalized difference vegetation index based on geographical detectors in Inner Mongolia. *Acta*
585 *Ecologica Sinica*. 2021, 12,1-3.
- 586 48. Li W, Huntsinger. China's grassland contract policy and its impacts on herder ability to benefit in Inner
587 Mongolia: tragic feedbacks. *Ecology and Society*. 2011,16, 1-12.
- 588 49. Zhang F, Nilsson C, Xu Z, Zhou G. Evaluation of restoration approaches on the Inner Mongolian Steppe based
589 on criteria of the Society for Ecological Restoration. *Land Degradation & Development*. 2020, 31, 285-296.
- 590 50. Chen K, Yang C, Bai L, Chen Y, Liu R, Chao L. Effects of natural and human factors on vegetation normalized
591 difference vegetation index based on geographical detectors in Inner Mongolia. *Acta Ecol. Sin*. 2021, 41, 4963-
592 4965.
- 593 51. Hao L, Sun G, Liu Y, Gao Z, He J, Shi T, Wu B. Effects of precipitation on grassland ecosystem restoration
594 under grazing exclusion in Inner Mongolia, China. *Landscape Ecology*. 2014, 29, 1657-1673.
- 595 52. Xie B, Jia X, Qin Z, Shen J, Chang Q. Vegetation dynamics and climate change on the Loess Plateau, China:
596 1982–2011. *Regional Environmental Change*. 2016, 16, 1583-1594.
- 597 53. Hao J, Lin Q, Wu T, Chen J, Li W, Wu X, Hu G, La Y. Spatial–temporal and driving factors of land use/cover

- 598 change in Mongolia from 1990 to 2021. *Remote Sensing*. 2023, 15, 1813.
- 599 54. Wang C, Wang S, Fu B, Lü Y, Liu Y, Wu X. Integrating vegetation suitability in sustainable revegetation for
600 the Loess Plateau, China. *Science of the Total Environment*. 2021, 759, 143572.
- 601 55. Tong S, Zhang J, Bao Y, Lai Q, Lian X, Li N, Bao Y. Analyzing vegetation dynamic trend on the Mongolian
602 Plateau based on the Hurst exponent and influencing factors from 1982–2013. *Journal of Geographical
603 Sciences*. 2018, 28, 595-610.
- 604 56. Su K, Liu H, Wang H. Spatial–temporal changes and driving force analysis of ecosystems in the Loess Plateau
605 Ecological Screen. *Forests*. 2022, 13, 54.
- 606 57. Bromley J, Brouwer J, Barker AP, Gaze SR, Valentine C. The role of surface water redistribution in an area of
607 patterned vegetation in a semi-arid environment, south-west Niger. *Journal of Hydrology*. 1997, 198, 1-29.
- 608 58. Yin H, Pflugmacher D, Li A, Li Z, Hostert P. Land use and land cover change in Inner Mongolia-understanding
609 the effects of China’s re-vegetation programs. *Remote Sensing of Environment*. 2018, 204, 918-930.